Mechanics and Differential Healing Outcomes of Small and Large Defect Injuries of the Tendon-Bone Attachment in the Rat Rotator Cuff

Anna Lia Sullivan [1], Ryan C. Locke[1], Rachel K. Klink[2], Connor C. Leek[1,3], Megan L. Killian[1,3]

[1]Department of Biomedical Engineering, University of Delaware, Newark, Delaware 19716

[2]Department of Physics and Engineering, Taylor University, Upland, Indiana 46989

[3]Department of Orthopaedic Surgery, Michigan Medicine, Ann Arbor, Michigan 48109

CORRESPONDING AUTHOR

Megan L. Killian, PhD

University of Michigan Medical School

Department of Orthopaedic Surgery

2021 BSRB, 109 Zina Pitcher Place, Ann Arbor, Michigan 48109

Phone: 734-936-256, E-mail: mlkillia@med.umich.edu

RUNNING TITLE

Healing of Differentially-Sized Enthesis Defects

AUTHOR CONTRIBUTIONS

ALS, RCL, RK, and MLK designed the experiments. ALS, RCL, and RK acquired the data. All authors analyzed and interpreted the data. ALS drafted the manuscript. RCL, RK, CCL, and MLK edited the manuscript. All authors have read and approved the final submitted manuscript.

ABSTRACT

The size of rotator cuff tears affects clinical outcomes following rotator cuff repair and is correlated with risk of re-injury. This study aimed to understand how defect size influences the structural and mechanical outcomes of the injured rotator cuff attachment *in vivo*. We used our previously established model of full-thickness injury of the rotator cuff tendon-bone attachment in Long Evans rats to compare differences in healing outcomes between small and large defects. Biomechanical properties, gross morphology, bone remodeling, and cell and tissue morphology were assessed at 3- or 8-weeks of healing. At the time of injury (no healing), large defects had decreased mechanical properties compared to small defects, and both defect sizes had decreased mechanical properties compared to intact attachments. The mechanical properties of the defect groups were comparable after 8-weeks of healing and significantly improved compared to no healing but failed to return to intact levels. Local bone volume at the defect site was higher in large compared to small defects on average and increased from 3- to 8-weeks. Contrastingly, bone quality, measured as bone volume percentage and trabecular morphometry, of the total epiphysis and greater tubercle decreased from 3- to 8-weeks of healing and these changes were not dependent on defect size. Qualitatively, we observed that large defects had increased disorganized collagen and neovascularization compared to small defects. In this study, we demonstrated that not only small but also large defects do not regenerate the mechanical and structural integrity of the intact rat rotator cuff attachment following healing *in vivo*. Statement of Clinical Significance: Our rat model of full-thickness rotator cuff tears may be beneficial to understand and prevent tear enlargement *in vivo.*

KEYWORDS

tendon, healing, attachment, biomechanics, animal model

INTRODUCTION

Small rotator cuff tears are one of the most common shoulder injuries.[1] These tears can limit normal function of the shoulder[2] and propagate into larger tears that require surgical repair.[3–6] The size of the initial tear prior to repair plays a critical role in post-operative healing and pain scores, as larger tears have been correlated with decreased tendon integrity, decreased range of motion, and an increased rate of shoulder osteoarthritis progression.[3,7,8] Small tears are often treated conservatively to eliminate pain. The outcomes of conservative treatments are highly variable,[4,9] and there is a high risk of tear propagation.[10] Larger tears commonly require surgical repair for functional reattachment of the injured tendon to bone.[11–15] Little is known about critical size of full-thickness tears in a single tendon that propagate into larger, more problematic tears *in vivo*. This study aimed to understand how defect size differentially affects healing of the attachment between tendon and bone in an *in vivo* rotator cuff injury model of full-thickness tears.

The rat is a commonly used animal model to study rotator cuff tears due to anatomical similarities to the human rotator cuff.[15] Previous studies using cadavers or animal models to study rotator cuff tears have shown that strain concentrations at the tendon-bone attachment are elevated with increasing tear size.[16–20] The majority of animal models used to study rotator cuff healing rely on complete tendon tears with sutured reattachment of tendon to its bony footprint to mimic the clinical scenario of rotator cuff repair.[21–31] Yet, few studies have investigated non-operative healing of small rotator cuff injuries *in vivo*.[18,19,32] While simulating the clinical scenario of rotator cuff tear and repair has benefits for understanding healing mechanisms of surgical repair, several unanswered questions remain regarding the regenerative capacity of the native tendon-bone attachment without surgical repair. We have previously observed that full-

thickness injuries of the tendon-bone attachment heal via fibrosis and result in significant reductions in bone quality.[19] Additionally, we have shown that non-healed small defects at the tendon-bone attachment lead to decreased strength and the formation of strain concentrations across the remaining intact attachment.[18] However, our previous studies only explored outcomes associated with healing and mechanical properties using a small defect and also did not compare mechanical outcomes following healing without repair.

In the present study, we created two different sized defects (small and large) at the rotator cuff tendon-bone attachment in the rat and assessed biomechanical properties and structural healing of these defects at different healing time points (no healing and 3- and 8-weeks of healing). We hypothesized that small and large defects would both result in fibrotic scar tissue formation, but that defect size matters; we expected that large defects would propagate into complete tears with evidence of tendon retraction and have diminished healing outcomes compared to small defects (i.e., decreased mechanical properties, bone quality, and organization).

METHODS

Surgical Procedure and Gross Morphology

Mature, Long Evans female rats (N = 32 total, n=8 per defect size for *in vivo* healing; n=10 per defect size for mechanical testing post-healing; and n=14 per defect size for non-healed injury mechanics, former breeders, 299±54g) were used under the accordance of the University of Delaware Institutional Animal Care and Use Committee. Under anesthesia (isoflurane carried by oxygen), rats underwent a bilateral surgical procedure to model small- and large full-thickness tears of the infraspinatus tendon-bone attachment using 0.3mm (small, ~33% damage) and 0.75mm (large, ~66% damage) punch biopsies (Robbins, Chatham, NJ USA).[18,19] A 2-cm

incision was made craniolateral to the glenohumeral joint and was followed by a horizontal incision to detach the deltoid from the acromion. A suture was passed under the acromion to elevate the scapula and expose the rotator cuff tendon-bone attachments. The infraspinatus tendon-bone attachment was located following internal shoulder rotation, the joint was stabilized, and the defect was created. Small or large punch biopsies were used at the center of the tendon-bone attachment to create full-thickness defects, which permeated and removed the fibrocartilaginous attachment and underlying cortical bone. The shoulder (left or right) that received a small or large defect was alternated between rats using controlled randomization. The muscle layer and skin were closed using simple interrupted resorbable sutures (5-0 Vicryl, Ethicon Inc., Somerville, New Jersey). Rats were given subcutaneous buprenorphine (0.05mg/kg) as analgesia and local bupivacaine hydrochloride (0.05mg/kg) as an anesthetic pre-operatively and postoperatively, respectively. Animals were closely monitored during recovery and twice daily for three days post-operatively. Rats were housed in cages (2 rats maximum per cage) with enrichment and unlimited access to food and water. Rats were euthanized via carbon dioxide asphyxiation and thoracotomy at 3- or 8-weeks post-surgery and entire shoulder complexes were dissected to visualize the infraspinatus attachment. Gross morphology images were taken using a digital camera (DSLR, Nikon). The 3-week time point was used to represent the inflammatory stage of the injury, and the 8-week time point was used to represent the remodeling stage (Figure 1, study design).

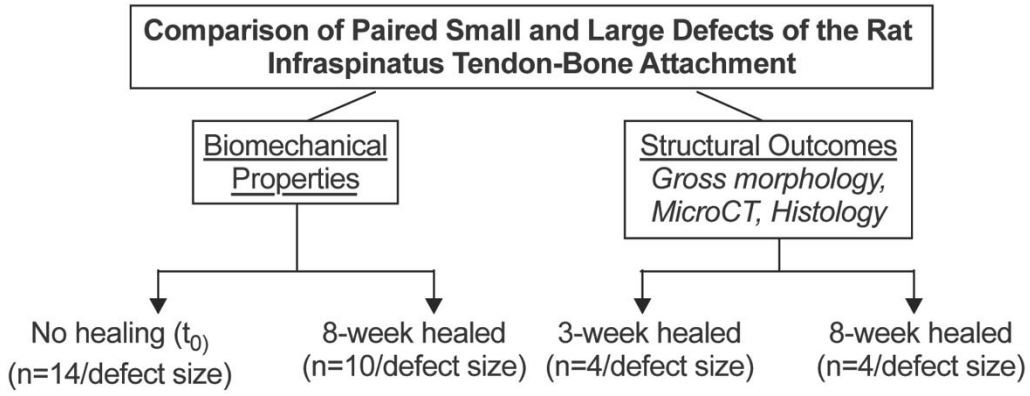

Figure 1. Study design. We compared the biomechanical properties and structural outcomes of paired small and large defects in the infraspinatus tendon-bone attachment of Long Evans rats *in vivo*. Biomechanical properties of small and large defects were assessed with no healing (t_0) and after 8-weeks of healing. The structural outcomes from gross morphology, micro-computed tomography (microCT), and histology were assessed after 3-weeks and 8-weeks of healing.

Biomechanics

Mechanical testing was performed to compare mechanical outcomes associated with two different defect sizes both with no healing (t_0, n=14 per defect size) and following a duration of healing (8-week time point, n=10 animals). A non-healed injury was mimicked in euthanized rats that were stored frozen until time of mechanical testing. Stereoscopic images were taken of the lateral and inferior sides of the attachment (DSLR, Nikon) and ImageJ was used to measure the width and thickness of these sides, respectively. The remaining intact attachment width was calculated by subtracting the defect diameter from the total attachment width for non-healed injuries. For non-healed injuries, the attachment was assumed to be rectangular to approximate cross-sectional area (CSA). For healed attachments, the CSA was assumed circular and measured from the lateral attachment width because there was a large circular scar around the healed attachments rather than rectangular “borders” that were more easily visualized in the non-healed

injuries. The humeral head was secured using steel wire (32AWG) to prevent growth plate failures. Distal humeri were potted in 1.5mL centrifuge tubes using polymethyl methacrylate (Ortho-Jet BCA, Lang Dental) or DP100 epoxy (3M, Scotch-Weld). Infraspinatus muscles were removed, and tendons were affixed in thin-film grips lined with PBS-soaked tissue paper (Kimwipes, Kimberly-Clark). Tendons were positioned in a materials test stand at 0-degree shoulder abduction. A 0.1N tare load was applied, and gauge length was recorded before uniaxial tensile tests began (Instron 5943, Norwood, MA). The test protocol was as follows: 10 preconditioning cycles from 0.025-0.075mm at a rate of 0.01mm/sec, followed by 90 seconds of rest, and ramp to failure at 0.01mm/sec. Ultimate load, stiffness, ultimate stress, strain at ultimate stress, Young's modulus, area under the curve (AUC) at ultimate stress, and AUC of the last five load-displacement preconditioning cycles (energy loss) were computed (MATLAB, Natick, MA).[18]

Microcomputed Tomography

Immediately following euthanasia and dissection, shoulders allocated for histology and micro-computed tomography (micro-CT) from 3- and 8-week time points (N = 8 rats total, 4 shoulders per defect size per time point) were fixed in 4% paraformaldehyde for 24-48 hours then scanned in air using micro-CT (1276 Skyscan; Bruker, 55kV source voltage, 200μA source current, 10.6μm image pixel size, 1200ms exposure). MicroCT images were reconstructed and aligned with DataViewer (Bruker). Bone morphometric properties for the defect area, greater tubercle, and proximal epiphysis were measured using Dragonfly software (Object Research Systems Inc., Figure 4A and S1). The defect area was defined following alignment of the X- and Y- planes for a normal view of the defect in the Z-planar view. Using the 2D painter tool in Dragonfly, a circle of diameter equal to the diameter of the punch biopsy was digitally painted

on the first slice where the full defect was observed in the z-plane. A cylinder-shaped region of interest (ROI) was then filled into the defect using a consistent cylinder height (370µm). Split and Otsu functions were used to separate mineral (bone) and non-mineral within this cylindrical ROI. Bone volume (BV) was divided by the total volume (TV) of the cylinder to calculate (BV/TV) ratio. Epiphyseal ROIs (total epiphysis and greater tubercle) were isolated using consistent anatomical landmarks, and the bone analysis function was used to fill holes smaller than 300µm in order to obtain the TV of the epiphysis. Trabecular and cortical bone were separated using the Kohler method (maximum trabecular thickness=150µm).[35] Total, trabecular, and cortical bone ROIs were isolated and analyzed using the Bone Analysis tool in Dragonfly (Figure 4A).

Histology

After microCT, samples were decalcified in Ethylenediaminetetraacetic acid (EDTA), paraffin embedded, and sectioned at 6µm thickness. Sections were stained with nuclear stain 4',6-diamidino-2-phenylindole (DAPI) and imaged at 3 individual locations within the attachment (0.024mm^2/image) to quantify cell number, aspect ratio (nAR), minor axis, major axis, equivalent diameter, perimeter, solidity, eccentricity, orientation and area of nuclei using a custom MATLAB code (Figure 5A-C).[36,37] Image replicates (3 per sample) were averaged per sample then used for statistical comparisons between defect groups. Hematoxylin & Eosin (H&E) was used to assess fibrosis, cellularity, and vascularity, and Picrosirius Red was used to assess collagen organization.

Statistical Analyses

Two-way ANOVA with repeated measures and Sidak's multiple comparison tests were used to compare mechanical outcomes, bone morphometry from microCT, and cell nuclear shape

of paired small and large defects at t_0 (mechanics only), 3- or 8-weeks of healing. All statistics were performed using Prism (version 8, GraphPad). Mechanical properties of intact attachments from Locke et al. were used for qualitative, not statistical, comparisons.[18]

RESULTS

All animals tolerated bilateral surgery well.

Mechanical Properties Increased with Healing

Four non-healed rats and one healed rat were excluded due to errors during data acquisition, dissection, and abnormal defect placement; therefore, n=10 per defect size were analyzed in the non-healed group, and n=9 per defect size were analyzed for the 8-week healed group. Two additional rats in the healed group were excluded from energy loss comparisons, but not load to failure comparisons, due to data acquisition errors during preconditioning.

Attachment CSA decreased as non-healed defect size increased, and following 8-weeks of healing, CSA was significantly increased for both defect groups (Figure 2A). In the non-healed group, ultimate load and stiffness were reduced and energy loss was higher but not significantly different in large compared to small defects (Figure 2B-D). Ultimate load and stiffness were reduced in both non-healed defect groups compared to intact attachments (Figure 2C-D), corroborating previous findings from our group.[18,19]

After 8-weeks of healing, both small and large defects had increased ultimate load and stiffness compared to non-healed defects; however, healed defects did not regain comparable properties to native, uninjured attachments (Figure 2C-D). Energy loss was reduced for healed defects compared to defects with no healing (Figure 2B). No differences were observed for Young's modulus, ultimate stress, AUC at ultimate stress, or strain at ultimate stress between defect sizes or healing duration (Table S1).

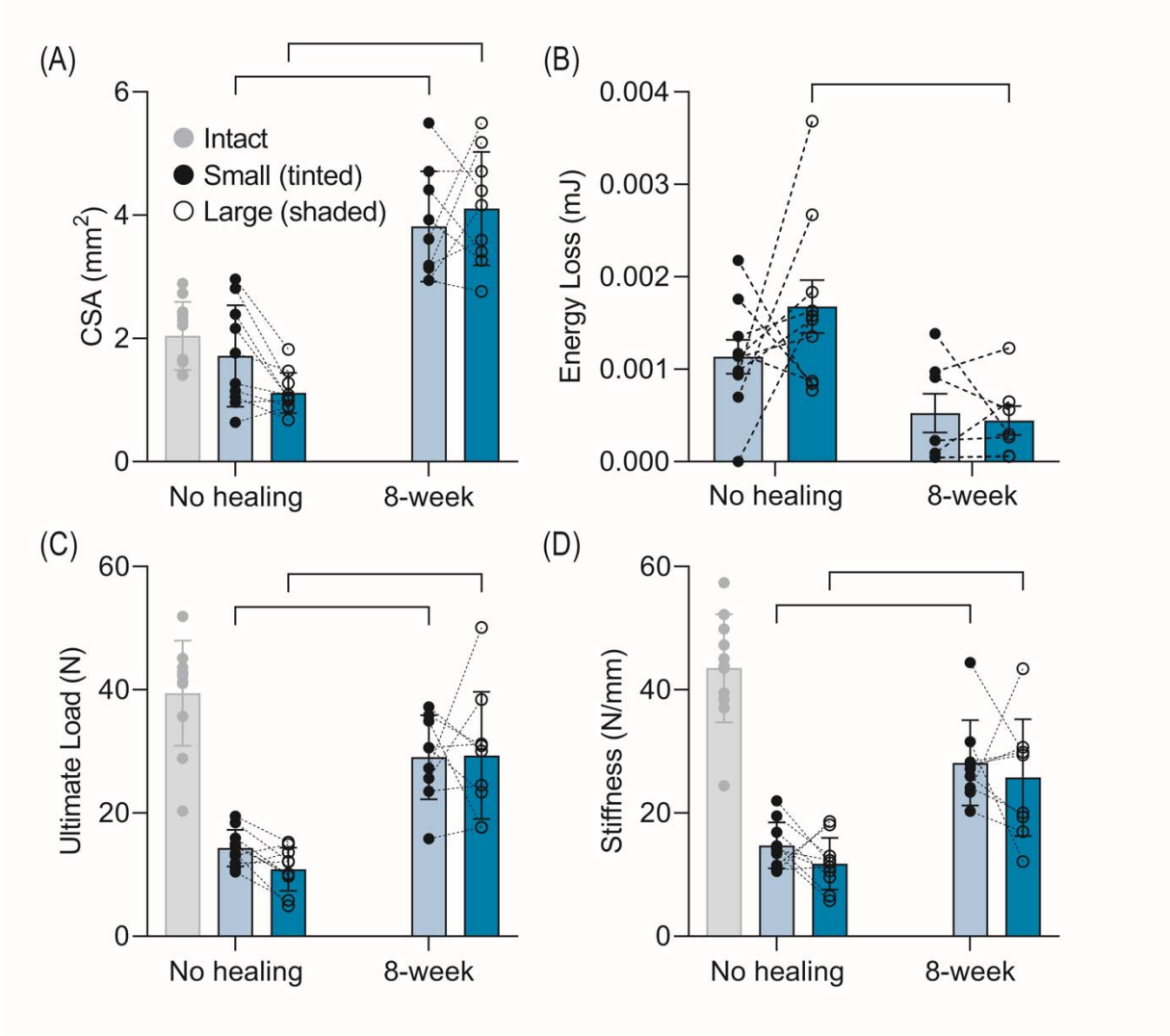

Figure 2. Critical defects that do not regenerate the intact mechanical properties of the tendon-bone attachment may be smaller than one-third of the attachment. (A) Cross sectional area (CSA), (B) energy loss, (C) ultimate load, and (D) stiffness for non-healed and healed small and large defects. Gray data: Intact attachment mechanical properties from Locke et al.[18] Bars: significant difference ($p<0.05$). Dashed lines: paired data points. Data are presented as mean ± standard deviation.

Gross Morphology and Bone Properties Were Affected by Defect Size and Healing Duration

From gross morphology, no tear propagation into complete tears or tendon retraction was observed for either defect size (Figure 3A-D), although increased neovascularization and fibrosis at the defect site were found for large compared to small defects (Figure 3A-D, white arrows). Large defects had increased fibrosis at 8-weeks compared to 3-weeks (Figure 3A-D).

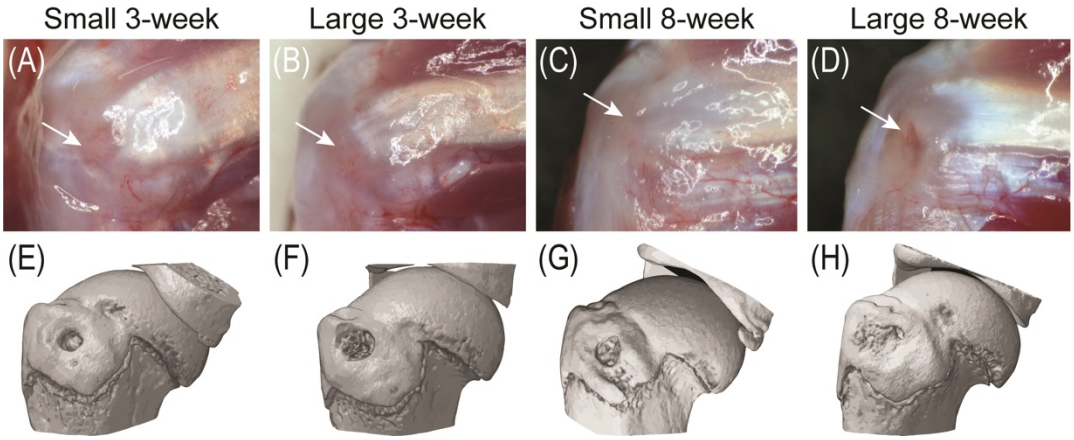

Additionally, we qualitatively observed less cortical bone for large defects compared to small defects at 3-weeks (Figure 3E-F).

Figure 3. Increased neovascularization, fibrosis, and cortical bone loss were observed for large defects compared to small defects. (A-D) Gross morphology of the defect sites (white arrows) at the time of dissection for small and large defects. (E-F) Representative micro-

computed tomography (microCT) 3-dimensional reconstructions of the defect site at the greater tubercle of the humeral head for small and large defects following 3- and 8-weeks of healing.

The amount of bone within the defect increased over time for both defect sizes (Fig 4) and bone volume fraction (BV/TV) was higher in large compared to small defects especially at 3-week (Figure 4B and S1, $p=0.02$). Conversely, trabecular morphometry of the humeral head (trabecular epiphysis, Figure 4C-D) and of the greater tubercle (Figure S2) decreased with increased healing time but did not vary between defect sizes. In the greater tubercle, trabecular separation (Figure 4E, $p < 0.01$) increased and trabecular thickness (Figure 4F, $p<0.01$) decreased from 3- to 8-weeks but did not differ between defect sizes.

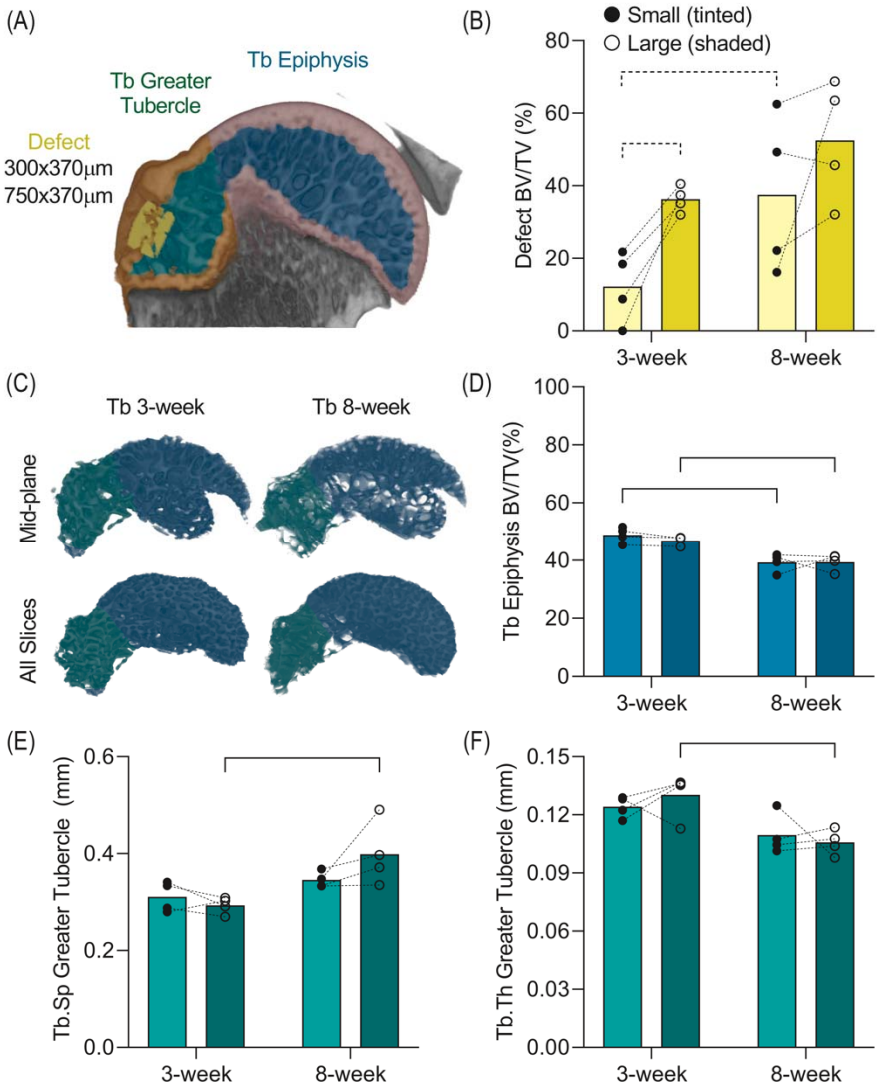

Figure 4. Bone properties increased locally at the defect site and decreased away from the defect site from 3-weeks to 8-weeks. (A) Representative microCT 3-dimensional (3D) reconstruction showing the regions of interest (ROIs) for trabecular (Tb) and cortical (Ct) bone segmentation and analysis: Tb epiphysis (blue), Ct epiphysis (purple), Tb greater tubercle (green), Ct greater tubercle (orange), and defect area (yellow). The epiphyseal ROIs (Tb and Ct) included data from all ROIs. (B) Defect area bone volume (BV) to tissue volume (TV) ratio (BV/TV) was increased in large compared to small defects overall. (C) Representative microCT

3D reconstruction at the mid-frontal plane and of the total epiphyseal Tb bone, showing reduced bone quality from 3- to 8-weeks. (D) Tb epiphysis BV/TV, (E) Tb separation (Sp) and (F) Tb thickness (Th) at the greater tubercle. Dashed bars: trend ($p<0.1$). Bars: significant difference ($p<0.05$). Dashed lines: paired data points. Data presented in bar charts are means.

Tissue Cellularity and Structure Were Mildly Different Between Defect Groups

Within the defect, cellularity was increased for large defects compared to small defects overall (Figure 5D, $p=0.02$). Large defects had significantly increased nuclear aspect ratio (Figure 5E) and eccentricity (Table S2) compared to small defects overall and at 8-weeks of healing (Figure 5E). The nuclear area (Figure 5F), equivalent diameter (Figure 5G), major axis, minor axis, and perimeter (Table S2) were all increased from 3- to 8-weeks of healing overall and in small defects from 3- to 8-weeks. The nuclear solidity and orientation were not affected by defect size or healing time (Table S2).

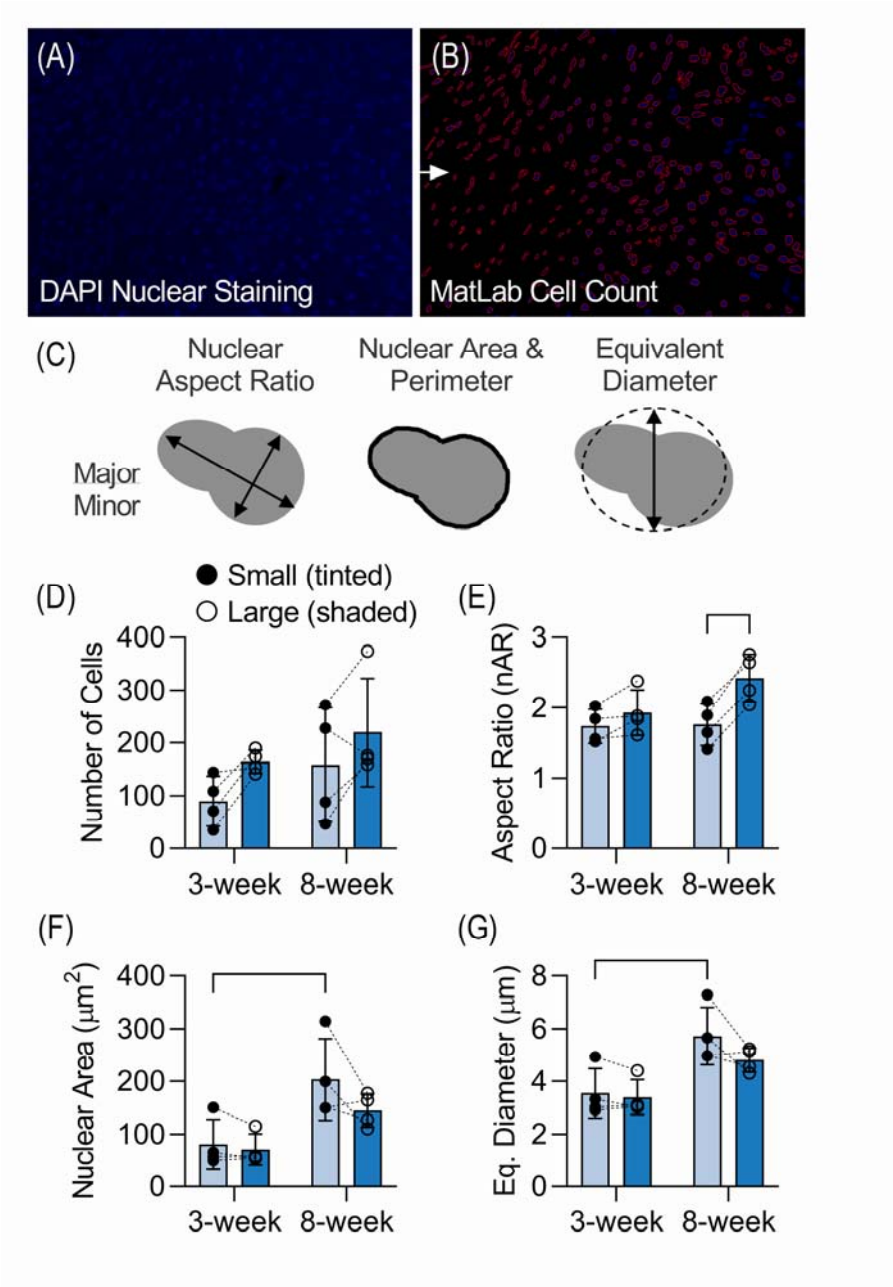

Figure 5. Cellularity and nuclear morphology were moderately impacted by defect size. (A) DAPI stained sections from within the injured attachment were imaged at 40x. Three technical replicates per biological sample were imaged and (B) a custom Matlab code was used to digitize and auto-segment the nuclei. The code was used to calculate and average (C) nuclear properties

for each technical and biological replicate. (D) Cellularity, (E) nuclear aspect ratio, (F) nuclear area, and (G) equivalent (Eq) diameter were measured and compared between defect sizes and healing durations. Bars: significant difference ($p<0.05$). Dashed lines: paired data points. Data are presented as mean ± standard deviation.

Both defect sizes had evidence of vascularity within the injured attachment (Figure 6A-B) and more vessels were observed for large defects compared to small defects at 3-weeks of healing (Figure 6B). Additionally, at 3-weeks, both defects had rounded nuclei within the injury region rather than elongated tendon fibroblasts, indicating the presence of macrophages or other cell populations (Figure 6A-B). From 3- to 8-weeks, both small and large defects had evidence of fibrosis surrounding the defect region and reduced appearance of vessels (Figure 6C-D). Qualitatively, we observed that small and large defects had mixed collagen organization after 3-weeks of healing (Figure 6E-F), while large defects resulted in more unorganized collagen

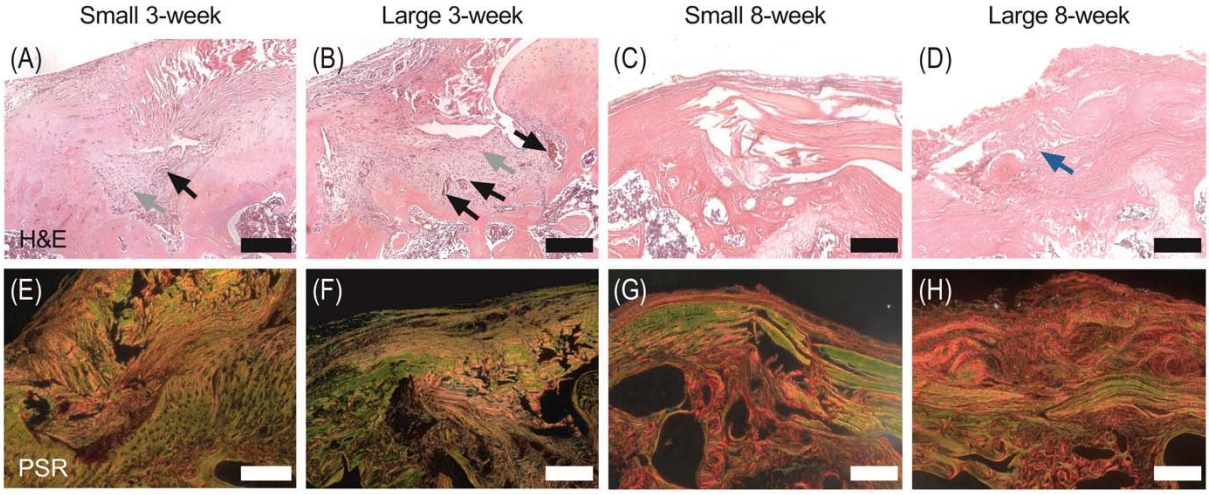

compared to small defects after 8-weeks of healing (Figure 6G-H).

Figure 6. Large defects had increased vasculature and scar tissue at 3-weeks and 8-weeks of healing, respectively. (A-D) Hematoxylin and Eosin (H&E) and (E-H) Picrosirius Red (PSR)

were used to assess tissue micro-structure and collagen organization. (A-B) At 3-weeks, both small and large attachments had evidence of vascularity (black arrows). Rounded nuclei (gray arrows) were observed at 3-weeks in both sized defects. (C-D) Following 8-weeks of healing, both defects had evidence of a fibrotic scar formation, with more observed in large defects (blue arrow). (E-F) Small and large defects had mixed organization of collagen after 3-weeks of healing. (G-H) Qualitatively, large defects compared to small defects resulted in more unorganized collagen at 8-weeks. Scale bars = 100µm.

DISCUSSION

In our study, we showed that the size of full-thickness rotator cuff defects did not play a significant role in mechanical outcomes, but did affect the gross morphology, bone morphometry, cellularity, and structure of the tendon-bone attachment. Surprisingly, and counter to our hypothesis, we observed similar mechanical properties of both defect sizes after 8-weeks of healing. Neither defect group regained the native mechanical properties of the healthy attachment, indicating that the attachment does not fully regenerate within 8-weeks following injury. Therefore, one-third or even less than one-third of the width of the tendon-bone attachment may be a critical defect in the rat rotator cuff. It is possible that a longer duration of healing could have led to restored mechanical properties comparable to the intact tendon-bone attachment. Additionally, differences in mechanical properties between defect sizes may have occurred at shorter durations of healing. Although we did not find a mechanical difference between defect sizes, we did observe several spatiotemporal differences in attachment bone properties, cellularity, and structure between defect sizes. We showed that the size of full-thickness rotator cuff defects was in part associated with healing outcomes.

Our model of full-thickness injury is similar to crescent-shaped tears that commonly present in the clinic and lead to tear propagation.[1,3] Tear propagation has been correlated with increased strain at the defect site.[20] In our injury model, although we observed multiple decreased mechanical properties between non-healed small and large defects compared to healthy attachments and have previously observed strain concentrations at the defect site[18], we did not observe tear propagation in either defect size following 8-weeks of healing *in vivo* under normal physiologic loading. Increased mechanical loading at the attachment to the point of overuse, however, may increase the likelihood of tear propagation even for small defects.[38,39] In our study, we did not challenge the injured attachment beyond the initiation of a defect. Physiologic loading in this study may have resulted in a protective healing response that prevented tear propagation into a complete tear and supported a similar increase in mechanical properties of both defects during healing.[40] Future studies could investigate the role of acute or repetitive loading on attachment damage and tear propagation by modulating muscle loading and attachment mechanobiology (e.g., treadmill running or muscle stimulation).[41]

Although we observed that the duration of injury affected healing outcomes more so than defect size, defect size lead to several differences in gross morphology, bone properties, cellularity, and attachment structure. Rotator cuff tears commonly lead to fibrosis and neovascularization,[19,24] and, in this study, we similarly observed a qualitative increase in fibrotic tissue and vessel formation with increased defect size. Additionally, various dynamic cell behaviors, such as migration, proliferation, and differentiation, as well as abnormal cell phenotypes, such as rounded cells, have been observed following tendon injury.[42,43] Notably, we observed a dynamic increase in cell number and structural characteristic of the attachment, including fibrosis and collagen organization, that were dependent both on defect size and healing

time, concurring with Lemmon et al. but contrasting other injury models.[19,30,31] A decrease in cell number and increased collagen organization may be observed with further healing duration, yet comparable tendon remodeling has been observed between 8- and 12-weeks,[44] suggesting that 8-weeks is an appropriate time point to assess attachment remodeling. These findings suggest that the rat attachment may adapt to the increased tear size in attempt to remodel the larger injury.

Nuclear aspect ratio (nAR) has been used previously as read out of mechanical force transmission experienced by cells, and changes in nuclear shape can trigger epigenetic changes and influence gene expression.[41,42,45,46] Previous studies have shown that tendon injury leads to an acute decrease in nAR compared to healthy tendons and that nAR increases with increased healing duration, indicating a mechanobiological response to injury and healing.[42] Interestingly, in this study, we observed changes in nAR of local fibroblasts that were dependent on injury size. Whether large defects result in increased tissue-scale strain compared to small defects and if the mechanical differences between defect sizes lead to differences in nAR remain unknown.[18] Alternatively, increased nAR, as well as nuclear area and equivalent diameter, in larger defects may suggest increased differentiation of local or extrinsic stem cells into fibroblasts.[42,47] Ultimately, we suggest that the dynamic nuclear changes observed in this study possibly developed from increased tissue-scale strain with increased defect size and/or altered mechanobiological force transmission with increased tissue remodeling. A further understanding of attachment mechanobiology may help to clarify these cellular adaptations to attachment defect size *in vivo*.[41,48]

Limitations

The use of this bilateral model allowed us to minimize the potential for abnormal loading on healing outcomes. However, a limitation to this study is that we did not quantify limb

preference during gait. Our model was beneficial as we utilized a bilateral defect which allowed us to pair our comparisons using biologically identical shoulders. Additionally, while decreased bone quality following acute tendon injury is common[25], the nature of our model likely contributed to a decrease in bone volume as the punch biopsy permeated through cortical bone.[18,19] Lastly, the use of an animal model to study rotator cuff tears has limitations when translating to humans due to differences in joint loading and healing. Although rats are a commonly used rotator cuff model, the use of rats in our study could potentially be a limiting factor. Rats have an increased propensity to heal with limited scar formation and are also quadrupeds that weight-bear on their forearms unlike humans. Although they perform overhead reaching and grasping, this is not identical to human biped motion.

It is important to understand how defect size can influence the mechanical and structural outcomes of attachment healing. The use of animal models to study the mechanical consequences and healing outcomes of critical defect size(s) can improve our preclinical understanding of early rotator cuff disease. This defect model can serve as a tool to understand the native healing process of full-thickness tears and as a testbed for preclinical testing of biomaterials that could be used to mitigate or delay surgical intervention of early rotator cuff disease.

ACKNOWLEDGEMENTS

Funding: Delaware Space Grant Consortium (NNX15AI19H), the UD Dare to be FIRST Research Experience for Undergraduates, the National Science Foundation Grant (1460757), the University of Delaware Doctoral Fellowship, the Eunice Kennedy Shriver National Institute Of Child Health & Human Development of the National Institutes of Health (K12HD073945), and the National Institute of General Medical Sciences of the National Institutes of Health

(P30GM103333). We would like to thank Francis Karani for animal handling and Dr. Gwen Talham for veterinary care.

REFERENCES

1. Matthewson G, Beach CJ, Nelson AA, et al. 2015. Partial Thickness Rotator Cuff Tears: Current Concepts. Advances in Orthopedics 2015:1–11.

2. Kartus J, Kartus C, Rostgård-Christensen L, et al. 2006. Long-term Clinical and Ultrasound Evaluation After Arthroscopic Acromioplasty in Patients With Partial Rotator Cuff Tears. Arthroscopy: The Journal of Arthroscopic & Related Surgery 22(1):44–49.

3. Randelli PS, Menon A, Nocerino E, et al. 2019. Long-term Results of Arthroscopic Rotator Cuff Repair: Initial Tear Size Matters. Am J Sports Med 47(11):2659–2669.

4. Maman E, Harris C, White L, et al. 2009. Outcome of Nonoperative Treatment of Symptomatic Rotator Cuff Tears Monitored by Magnetic Resonance Imaging: The Journal of Bone and Joint Surgery-American Volume 91(8):1898–1906.

5. Kim Y-K, Jung K-H, Kim J-W, et al. 2017. Factors Affecting Rotator Cuff Integrity After Arthroscopic Repair for Medium-sized or Larger Cuff Tears: A Retrospective Cohort Study. Journal of Shoulder and Elbow Surgery .

6. Reilly P, Amis AA, Wallace AL, Emery RJH. 2003. Supraspinatus tears: propagation and strain alteration. Journal of Shoulder and Elbow Surgery 12(2):134–138.

7. Kim HM, Dahiya N, Teefey SA, et al. 2010. Relationship of Tear Size and Location to Fatty Degeneration of the Rotator Cuff. The Journal of Bone and Joint Surgery-American Volume 92(4):829–839.

8. Mall NA, Kim HM, Keener JD, et al. 2010. Symptomatic Progression of Asymptomatic Rotator Cuff Tears: A Prospective Study of Clinical and Sonographic Variables. The Journal of Bone and Joint Surgery-American Volume 92(16):2623–2633.

9. Moosmayer S, Lund G, Seljom US, et al. 2014. Tendon Repair Compared with Physiotherapy in the Treatment of Rotator Cuff Tears: A Randomized Controlled Study in 103 Cases with a Five-Year Follow-up. The Journal of Bone and Joint Surgery-American Volume 96(18):1504–1514.

10. Cho NS, Rhee YG. 2009. The Factors Affecting the Clinical Outcome and Integrity of Arthroscopically Repaired Rotator Cuff Tears of the Shoulder. Clin Orthop Surg 1(2):96.

11. Chillemi C, Petrozza V, Garro L, et al. 2011. Rotator Cuff Re-Tear or Non-Healing: Histopathological Aspects and Predictive Factors. Knee Surg Sports Traumatol Arthrosc 19(9):1588–1596.

12. Hug K, Gerhardt C, Haneveld H, Scheibel M. 2015. Arthroscopic Knotless-Anchor Rotator Cuff Repair: A Clinical and Radiological Evaluation. Knee Surg Sports Traumatol Arthrosc 23(9):2628–2634.

13. Kim HM, Caldwell J-ME, Buza JA, et al. 2014. Factors Affecting Satisfaction and Shoulder Function in Patients with a Recurrent Rotator Cuff Tear: The Journal of Bone and Joint Surgery-American Volume 96(2):106–112.

14. Robinson PM, Wilson J, Dalal S, et al. 2013. Rotator Cuff Repair in Patients Over 70 Years of Age: Early Outcomes and Risk Factors Associated With Re-Tear. The Bone & Joint Journal 95-B(2):199–205.

15. Soslowsky L, Carpenter JE, DeBano CM, et al. 1996. Development and Use of an Animal Model for Investigations on Rotator Cuff Disease. J. Shoulder Elbow Surg. 5(5):10.

16. Miller RM, Fujimaki Y, Araki D, et al. 2014. Strain Distribution Due to Propagation of Tears in the Anterior Supraspinatus Tendon. J. Orthop. Res. 32(10):1283–1289.

17. Miller RM, Thunes J, Musahl V, et al. 2018. Effects of Tear Size and Location on Predictions of Supraspinatus Tear Propagation. Journal of Biomechanics 68:51–57.

18. Locke RC, Peloquin JM, Lemmon EA, et al. 2017. Strain Distribution of Intact Rat Rotator Cuff Tendon-to-Bone Attachments and Attachments With Defects. Journal of Biomechanical Engineering 139(11):111007.

19. Lemmon EA, Locke RC, Szostek AK, et al. 2018. Partial-Width Injuries of the Rat Rotator Cuff Heal with Fibrosis. Connective Tissue Research 59(5):437–446.

20. Andarawis-Puri N, Ricchetti ET, Soslowsky LJ. 2009. Rotator Cuff Tendon Strain Correlates With Tear Propagation. Journal of Biomechanics 42(2):158–163.

21. Killian ML, Cavinatto LM, Ward SR, et al. 2015. Chronic Degeneration Leads to Poor Healing of Repaired Massive Rotator Cuff Tears in Rats. Am J Sports Med 43(10):2401–2410.

22. Chen M, Shetye SS, Huegel J, et al. 2018. Biceps Detachment Preserves Joint Function in a Chronic Massive Rotator Cuff Tear Rat Model. Am J Sports Med 46(14):3486–3494.

23. Smietana MJ, Moncada-Larrotiz P, Arruda EM, et al. 2017. Tissue-Engineered Tendon for Enthesis Regeneration in a Rat Rotator Cuff Model. BioResearch Open Access 6(1):47–57.

24. Sato EJ, Killian ML, Choi AJ, et al. 2014. Skeletal Muscle Fibrosis and Stiffness Increase After Rotator Cuff Tendon Injury and Neuromuscular Compromise in a Rat Model. J. Orthop. Res. 32(9):1111–1116.

25. Thangarajah T, Henshaw F, Sanghani-Kerai A, et al. 2017. Supraspinatus Detachment Causes Musculotendinous Degeneration and a Reduction in Bone Mineral Density at the Enthesis in a Rat Model of Chronic Rotator Cuff Degeneration. Shoulder & Elbow 9(3):178–187.

26. Gimbel JA, Van Kleunen JP, Mehta S, et al. 2004. Supraspinatus Tendon Organizational and Mechanical Properties in a Chronic Rotator Cuff Tear Animal Model. Journal of Biomechanics 37(5):739–749.

27. Barton ER, Gimbel JA, Williams GR, Soslowsky LJ. 2005. Rat Supraspinatus Muscle Atrophy After Tendon Detachment. J. Orthop. Res. 23(2):259–265.

28. Yonemitsu R, Tokunaga T, Shukunami C, et al. 2019. Fibroblast Growth Factor 2 Enhances Tendon-to-Bone Healing in a Rat Rotator Cuff Repair of Chronic Tears. Am J Sports Med 47(7):1701–1712.

29. Bell R, Taub P, Cagle P, et al. 2015. Development of a Mouse Model of Supraspinatus Tendon Insertion Site Healing. J. Orthop. Res. 33(1):25–32.

30. Galatz LM, Sandell LJ, Rothermich SY, et al. 2006. Characteristics of The Rat Supraspinatus Tendon During Tendon-To-Bone Healing After Acute Injury. J. Orthop. Res. 24(3):541–550.

31. Kanazawa T, Gotoh M, Ohta K, et al. 2016. Histomorphometric and Ultrastructural Analysis of the Tendon-Bone Interface After Rotator Cuff Repair in a Rat Model. Sci Rep 6(1):33800.

32. Schwartz AG, Galatz LM, Thomopoulos S. 2017. Enthesis Regeneration: A Role for Gli1+ Progenitor Cells. Development :dev.139303.

36. David MA, Smith MK, Pilachowski RN, et al. 2017. Early, Focal Changes in Cartilage Cellularity and Structure Following Surgically Induced Meniscal Destabilization in the Mouse. Journal of Orthopaedic Research 35(3):537–547.

37. Locke RC, Lemmon EA, Dudzinski E, et al. 2020. Photobiomodulation Does not Influence Maturation and Mildly Improves Functional Healing of Mouse Achilles Tendons. Journal of Orthopaedic Research .

38. Tucker JJ, Riggin CN, Connizzo BK, et al. 2016. Effect of overuse-induced tendinopathy on tendon healing in a rat supraspinatus repair model. Journal of Orthopaedic Research 34(1):161–166.

39. Parks AN, McFaline Figueroa J, Coogan A, et al. 2017. Supraspinatus tendon overuse results in degenerative changes to tendon insertion region and adjacent humeral cartilage in a rat model. Journal of Orthopaedic Research 35(9):1910–1918.

40. Kurdziel MD, Davidson A, Ross D, et al. 2019. Biomechanical properties of the repaired and non-repaired rat supraspinatus tendon in the acute postoperative period. Connective Tissue Research 60(3):254–264.

41. Leek CC, Soulas JM, Sullivan AL, Killian ML. 2020. Using Tools in Mechanobiology to Repair Tendons. Current Tissue Microenvironment Reports 1(2):31–40.

42. Freedman BR, Rodriguez AB, Leiphart RJ, et al. 2018. Dynamic Loading and Tendon Healing Affect Multiscale Tendon Properties and ECM Stress Transmission. Sci Rep 8(1):10854.

43. Howell K, Chien C, Bell R, et al. 2017. Novel Model of Tendon Regeneration Reveals Distinct Cell Mechanisms Underlying Regenerative and Fibrotic Tendon Healing. Sci Rep 7(1):45238.

44. Thomopoulos S, Williams GR, Soslowsky LJ. 2003. Tendon to bone healing: differences in biomechanical, structural, and compositional properties due to a range of activity levels. Journal of Biomechanical Engineering 125(1):106–113.

45. Arnoczky SP, Lavagnino M, Egerbacher M, et al. 2008. Loss of Homeostatic Strain Alters Mechanostat “Set Point” of Tendon Cells In Vitro. Clin Orthop Relat Res 466(7):1583–1591.

46. Sarasa-Renedo A, Chiquet M. 2005. Mechanical Signals Regulating Extracellular Matrix Gene Expression in Fibroblasts. Scand J Med Sci Sports 15(4):223–230.

47. Sawadkar P, Player D, Bozec L, Mudera V. 2020. The mechanobiology of tendon fibroblasts under static and uniaxial cyclic load in a 3D tissue engineered model mimicking native extracellular matrix. J Tissue Eng Regen Med 14(1):135–146.

48. Killian ML, Cavinatto L, Galatz LM, Thomopoulos S. 2012. The role of mechanobiology in tendon healing. J Shoulder Elbow Surg 21(2):228–237.